

Surface modification by high-energy heavy ion irradiation in various crystalline ZnO facets

A. Jagerová^{a,b}, R. Mikšová^a, O. Romanenko^a, Z. Sofer^c, P. Slepíčka^d, Jan Mistrík^{e,f}, A. Semerádtová^g, A. Macková^{a,b}

^a*Nuclear Physics Institute of the Czech Academy of Sciences, v. v. i., 250 68 Řež, Czech Republic*

^b*Department of Physics, Faculty of Science, J.E. Purkinje University, 400 96 Ústí nad Labem, Czech Republic*

^c*Department of Inorganic Chemistry, University of Chemistry and Technology in Prague, 166 28 Prague, Czech Republic*

^d*Department of Solid State Engineering, University of Chemistry and Technology in Prague, 166 28 Prague, Czech Republic*

^e*Institute of Applied Physics and Mathematics, Faculty of Chemical Technology, University of Pardubice, 532 10 Pardubice, Czech Republic*

^f*Center of Materials and Nanotechnologies, Faculty of Chemical Technology, University of Pardubice, 530 02 Pardubice, Czech Republic*

^g*Department of biology, Faculty of Science, J.E. Purkinje University, 400 96 Ústí nad Labem, Czech Republic*

1. Abstract

Nowadays, self-assembled surface nanoscale structures on various ZnO-facets are excellent templates for the deposition of semiconductor quantum dots as well as the tuned surface morphology can lead to the tuned surface optical transparency. In this work, we modified surface of *c-plane*, *m-plane* and *a-plane* single crystal ZnO facets by high-energy W ion irradiation with energy 27 MeV to follow surface morphology aspects and optical properties evolution. Ion fluences were kept in range $5 \times 10^9 \text{ cm}^{-2}$ to the $5 \times 10^{11} \text{ cm}^{-2}$ starting from a single ion implantation regime to the regime of overlapping impacts to see various regime of surface modification. Rutherford backscattering spectroscopy in channelling regime (RBS-C) and Raman spectroscopy identified slightly growing Zn-sublattice disorder in the irradiated samples with more significant enhancement for the highest irradiation fluence. Simultaneously, the strong suppression of main Raman modes and propagation of modes corresponding to the polar Zn-O vibrations indicates disorder mainly in O-sublattice in non-polar facets. The surface morphology, analysed by atomic force microscopy (AFM), shows significant change after the ion irradiation. The *c-plane* and *a-plane* ZnO exhibit formation of

small grains on the surface which density increase with irradiation fluence. The *m-plane* ZnO forms sponge-like surface for lower fluences and grains for the highest fluence. The surface roughness itself increase with irradiation fluence as was observed from AFM measurement as well from the spectroscopic ellipsometry (SE) analysis. The optical response of irradiation process was studied by SE and photoluminescence. Damage caused by high energy irradiation leads to the non-radiative processes and to the suppression of near band edge peak as well as deep level emission peak in photoluminescence spectra. Refraction index n and extinction coefficient k , determined by SE, exhibit blurring of features corresponding to the particular exciton states and slight decrease of both optical constants in optical band gap region due to growing crystal damage. This decrease was most pronounced in polar *c-plane* ZnO facet.

2. Keywords

ZnO, high energy irradiation, RBS, optical characterisation, surface modification

3. Introduction

Swift heavy ion (SHI) irradiation becomes an attractive way for nanomaterial design and nanostructuring fabrication. The example of SHI modification includes nanoparticles shaping and elongation of their lateral dimension or ion-track engineering where SHI's certain impact may be used for modification of optical properties or as waveguides applied in optics and bionics. [1–3] SHI irradiation process is specific due to prevailing ion-interaction with solid matter with prevalence of electron stopping forces (energy lost per unit length of the trajectory $S_e = (dE/dz)$ due to electron excitation). For SHI, the electron stopping forces are typically above a value of threshold for the latent track formation, which is for most of the related crystalline materials such as GaN, GaAs or Si in a range 15 - 36 keV/nm.[4,5] The huge energy transfer through the electron excitation results in localized melting and causes partial re-crystallization or matrix amorphization along the ion path. At the sample surface, the large amount of kinetic energy is rapidly transferred to the material causing the outburst of the knock-out near surface atoms. This leads to the modification of the surface morphology, change in the surface roughness and creation of hillocks or craters which can affects surface activity and physical properties. [6,7]

Surface patterning of solids with heavy ion bombardment is common low cost and effective way to enhance effective surface area, prepare surfaces with particular shapes or specify its periodicity. [8–10] It was possible to achieved diverse types self-organised periodic surface

structures such as nanodots arrays, nanoholes, hillocks or ripples by ion bombardment of solids realized at normal or grazing incidence angle. [11–13] The patterning of the surfaces with features of particular size and shape or preparation of ripples with control of its amplitude is a versatile method to control charge transfer in surface structures and tailor optical properties of semiconductors. [14,15] Simultaneously, the impact of single ion implantation on the crystalline semiconductor (Si, SiC, ZnO) nanostructuring has been shown to be prospective in control of the particular defect creation, functionalise deep-level impurities or formation of single centres with possible application in quantum computing. [16–18]

The ion irradiation is effective way for nanostructuring of wide band gap semiconductors such as ZnO and tailoring their optical properties. The surfaces of ZnO films and single crystals were already successfully modified by use of pulsed lasers or ion bombardment. [19,20] The uniformly distributed nano-hillocks were prepared on the relatively smooth surface of ZnO films by Au ion irradiation with energy 75 MeV as a consequence of energy transfer of thermal spike. [21] Further, it was proved that ZnO single crystal nano-rippled with Ar ion bombardment exhibit certain level of optical damage and change in optical constants. [22] However, the origin of optical signature of crystalline ZnO induced by SHI surface patterning is not completely understood.

Recently, the damage accumulation asymmetry was shown for various ZnO facets modified by low, medium and high energy ion irradiation. [23–25] The effect of ZnO crystallographic facet influence on the synthesis of surface nanostructures was simultaneously observed in case of SHI Au-ion surface nanostructuring. [26] To follow defect creation caused by SHI in the low ion fluence regime, where individual ion impact is expected, the surfaces of polar and non-polar ZnO crystallographic facets were modified by high-energy ion irradiation with heavy transition metals (W). Further, the focus should be given to the understanding to the connection between prepared nanostructures and its optical properties.

4. Experiment

The hydrothermally grown single-crystalline ZnO substrates were purchased from the company Crystal GmbH in Germany. For the experiment were used ZnO substrates (10 x 10 x 1 mm³) with three different crystallographic facets polar *c-plane* (0001) and two non-polar facets *a-plane* (11-20) and *m-plane* (10-10). All samples were irradiated by heavy energetic

W^+ ions produced by tandem accelerator Tandetron. The irradiation was carried out at 7° in off-axis mode to minimize channelling effect and enhanced surface modification.

The low ion irradiation fluence, set in a range 5×10^9 up to $5 \times 10^{11} \text{ cm}^{-2}$, was kept in a regime close to single ion irradiation for the lowest ion fluence and in overlapping impacts at the highest ion irradiation fluence to synthesize surface nanostructures. The estimated impact on average area $1 \times 1 \text{ } \mu\text{m}^2$ is 50 atoms for fluence $5 \times 10^9 \text{ cm}^{-2}$. For fluences $5 \times 10^9 \text{ cm}^{-2}$ and $5 \times 10^{11} \text{ cm}^{-2}$ it is 10 times and 100 times more, respectively. To keep the ion fluence in single ion irradiation regime, the ion beam current has to be precisely controlled during the ion irradiation. The irradiation system was accompanied with movable Faraday cup and electronics adapted for measurement of low currents from several fA up to several nA. The stability of the beam current was measured about half an hour before the ion irradiation itself and immediately after irradiation, which takes several minutes.

The energy of W^+ was set to 27 MeV when the electron stopping forces were determined as 8 keV/nm in surface region according to SRIM [27] simulations. SRIM software based on Monte Carlo calculations provides the full damage cascade simulation of ion path seen at the Figure 1a and calculation of electron and nuclear stoppings shown at Figure 1b. It can be expected that electron stopping threshold for continuous latent track formation by SHI in crystalline ZnO will be higher or comparable to the values given for similar GaN (15 keV/nm).[4] Nevertheless, the surface modification can be achieved even with electron stopping energies under this threshold. [28] In the subsurface region, energetic ions maintain straight trajectory with lower number of recoils corresponding to the modification mainly by electrons in contrast to the deeper buried layer (projected range of ions $3.75 \text{ } \mu\text{m}$) with prevailing nuclear stopping accompanied by dense collision cascade.

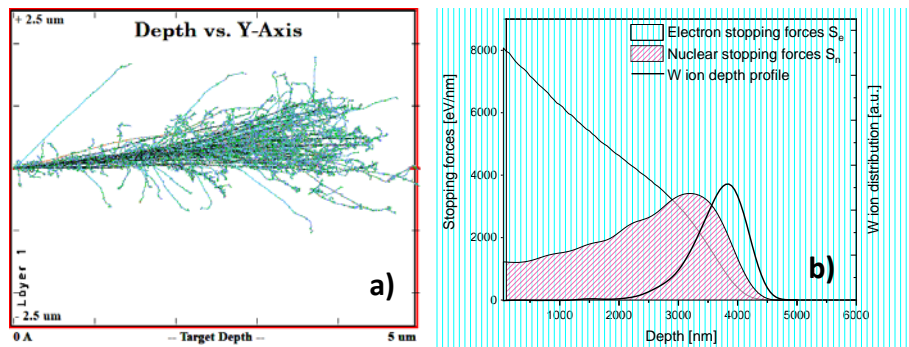


Figure 1 – Monte Carlo simulations by program SRIM of full damage cascade in ZnO crystal irradiated with 27 MeV W ions presented at a) and corresponding electron and nuclear stoppings with W distribution in depth at b)

Rutherford backscattering spectroscopy in channelling regime (RBS-C) was used for structural characterisation in sub surface region. For RBS-C was used He^+ ion beam with energy 2 MeV with information depth up to 1.2 μm . The overall information about the structural changes after ion irradiation was supplemented by Raman spectroscopy to study response of Zn and O sub-lattice to accumulated disorder. Surface morphology modification and nanostructuring was followed by Atomic Force microscopy (AFM).

For Raman spectroscopy was used a Renishaw InVia Raman confocal microscope with a Nd:YAG laser (532 nm). Output power was 50 mW. Detection of Raman spectra was carried out with a 100x objective and a TE-cooled CCD camera. The change in surface morphology was investigated by AFM device Integra (NT-MDT) in tapping mode. The measurement was realized with diamond probes with resonant frequency 190-325 kHz and spring constant of 5.5 – 22.5 N/m.

The micro-photoluminescence and optical ellipsometry were utilized for analysis of the optical response of the single-crystalline ZnO before and after modification by heavy energetic ions. The micro-photoluminescence spectra were measured using a HeCd laser (325 nm, 22 mW). The spectra were detected with TE-cooled CCD camera using a 20 \times NUV-long working distance objective. Ellipsometry spectra were acquired in the range 0.7 – 6.5 eV by VASE ellipsometer (Woollam). Angle of incidence span broad interval 40°– 80° to analyse optical anisotropy of both pristine and irradiated ZnO surfaces. Non-polar a-plane and m-plane facets, with the optical axis lying in-plane, were measured in two sample orientations where the optical axis was parallel and perpendicular with respect to the incidence plane, respectively. This enabled determination of both ordinary and extraordinary complex refractive indices. Measurements on polar c-plane facet, with the optical axis perpendicular to the surface, provided only average optical constants. In addition to the ellipsometry data also reflectance spectra were recorded for nearly normal incidence (with the same instrument) and both analysed simultaneously by WVASE32 software. Backside of the samples were grounded, therefore only single interface (sample surface) was considered in numerical data treatment. ZnO dielectric function was parameterized by Tanguy [29] and three Gauss oscillators to cover excitonic and interband electronic transitions in ZnO.

5. Results

5.1. Structural characterization measured by RBS-C and Raman spectroscopy

RBS-C results do not exhibit significant modification in the sub-surface region up to $1.38\ \mu\text{m}$ (Figure 2a-c) for all used ZnO facets. The slight crystal damage corresponds to the modification by energetic ions in prevailing electron stopping regime with low dense collision cascade. However, an asymmetry between used facets is visible even from RBS-C spectra. The *a-plane* ZnO shows the highest resistivity due to radiation damage represented by a minimal change in a backscattered ion yield measured by RBS-C for all used irradiation fluences. In contrast to the *a-plane*, the radiation resistance of *m-plane* ZnO is weaker [23,24] and the yield of backscattered ions slightly increases even after irradiation with the lowest fluence $5 \times 10^9\ \text{cm}^{-2}$. Modification of *c-plane* is appreciable mainly after modification with the highest irradiation fluence $5 \times 10^{11}\ \text{cm}^{-2}$. For the lower fluences only slight change in backscattered ion yields have been observed.

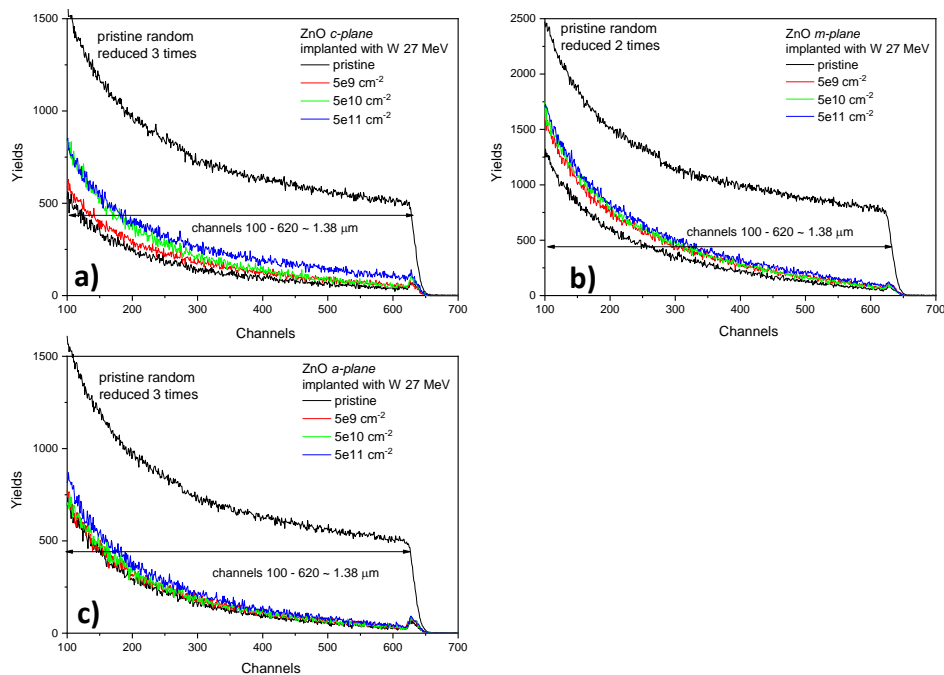


Figure 2 - RBS channelling spectra for ZnO implanted with W ions with energy 27 MeV for a) *c-plane*, b) *m-plane* and c) *a-plane* crystallographic orientation

Further, we followed the normalized minimal yield as a feature which tells us about Zn sub-lattice disorder. The normalized yield χ_{\min} has been determined from the RBS-C spectra as a ratio between aligned and random yield in the region of interest 100 - 620 channel which corresponds to the depth $1.38\ \mu\text{m}$ investigated by RBS with $2\ \text{MeV}\ \text{He}^+$ ion beam and is summarized in Table 1. The χ_{\min} in a range 100 – 620 channel was determined for the pristine

samples as well. Channelling in a depth is influenced by additional effects such as multi-scattering, thus dechannelling effect in the higher depths is more pronounced, so the normalized yields for the pristine samples evaluated in the whole region of interest are higher than generally reported values around 3 - 4 % [30,31] determined in a region just beyond the surface peak. The χ_{\min} analysis confirmed the lowest increase of Zn-sublattice disorder in *a-plane* ZnO crystals observed also in [26]. For lower irradiation fluences the χ_{\min} values stay nearly the same as for pristine sample and the change is in a range of the measurement uncertainty. For the highest fluence the χ_{\min} increase from 7.8 up to 10.1 % in *a-plane*. The normalized yield in the region of interest of *m-plane* ZnO is higher than 19 % even for lowest fluence $5 \times 10^9 \text{ cm}^{-2}$ and gradually increases with the W-ion irradiation fluence which represents the highest Zn atom disorder induced by the W-ion irradiation from all studied crystallographic orientations. In case of *c-plane* ZnO, the change in χ_{\min} is negligible for the lowest fluence. Further increase of the ion irradiation fluence leads to the enhancement of the normalized yield from 6.8 % (pristine) to the 9.8 % and 11.7 % for the fluences $5 \times 10^{10} \text{ cm}^{-2}$ and $5 \times 10^{11} \text{ cm}^{-2}$, respectively.

Table 1 - Normalized yield χ_{\min} of backscattered He⁺ ion for various ZnO facets modified by W⁸⁺ ions with energy 27 MeV

| Irradiation fluence [cm⁻²] | χ_{\min} <i>c-plane</i> [%] | χ_{\min} <i>m-plane</i> [%] | χ_{\min} <i>a-plane</i> [%] |
|--|--|--|--|
| Pristine | 6.8 ± 2 | 15.2 ± 2 | 7.8 ± 2 |
| 5×10^9 | 8.1 ± 2 | 19.4 ± 2 | 8.8 ± 2 |
| 5×10^{10} | 9.8 ± 2 | 20.1 ± 2 | 8.8 ± 2 |
| 5×10^{11} | 11.7 ± 2 | 21.5 ± 2 | 10.1 ± 2 |

ZnO crystallizes in a wurtzite structure which represents several main peaks in Raman spectra as it is seen in Figure 3a-c. The most intensive modes E_2^{high} and E_2^{low} situated at 100 and 430 cm^{-1} are connected to the vibration state of non-polar bonds of O and Zn sub-lattice, respectively. Its intensity is strongly affected by the changes in crystal structure and reflects the crystal quality. Further, the wurtzite ZnO shows double degenerated $2E_2$ mode at 203 cm^{-1} and mode referred as ($E_2^{\text{high}} - E_2^{\text{low}}$) at 330 cm^{-1} which is assigned to the second order Raman scattering. In case of non-polar ZnO facets *m-plane* and *a-plane* (Figure 3b,c), polarity of Zn-O bonding induces propagation of A_1 and E_1 modes splitted to the longitudinal and transversal modes $A_1(\text{TO})$, $E_1(\text{TO})$ at 375 and 410 cm^{-1} , $A_1(\text{LO})$, $E_1(\text{LO})$ at 540 cm^{-1} and 575 cm^{-1} , respectively. The A_1 and E_1 modes are highly sensitive to the intrinsic defects such as oxygen vacancies or zinc interstitials directed along the basal plane for A_1 mode and perpendicular to the basal plane for E_1 . [32,33]

In overall, Raman spectra of *c-plane* ZnO samples do not show significant modification of E_2^{high} and E_2^{low} peaks caused by W-ion irradiation. From the Figure 3a, it is clear that the lowest fluence does not cause any difference in spectra of the irradiated sample in comparison to the pristine ZnO *c-plane*. Higher W-ion irradiation fluence $5 \times 10^{10} \text{ cm}^{-2}$ supports propagation of modes $A_1(\text{LO})$ and $E_1(\text{LO})$ and their intensity increases with further enhancement of the W-ion irradiation fluence. Additionally, we can observe the distinct structural modification in non-polar ZnO facets exhibited with the significant decrease of E_2^{high} and E_2^{low} . Irradiation of *m-plane* with lowest fluence does not leads to a change in Raman spectra but enhancement of irradiation fluence results in gradual lowering of E_2 . The irradiation with the highest fluence also results in appearance of $A_1(\text{LO})$ and $E_1(\text{LO})$ modes. The Raman spectrum of the ZnO *a-plane* irradiated with fluence $5 \times 10^9 \text{ cm}^{-2}$, presented at Figure 3c, is not affected by W-ion irradiation, however the spectra of modified *a-plane* ZnO above this fluence exhibit rapid reduction of E_2 modes with the rise of $A_1(\text{LO})$ and $E_1(\text{LO})$ modes.

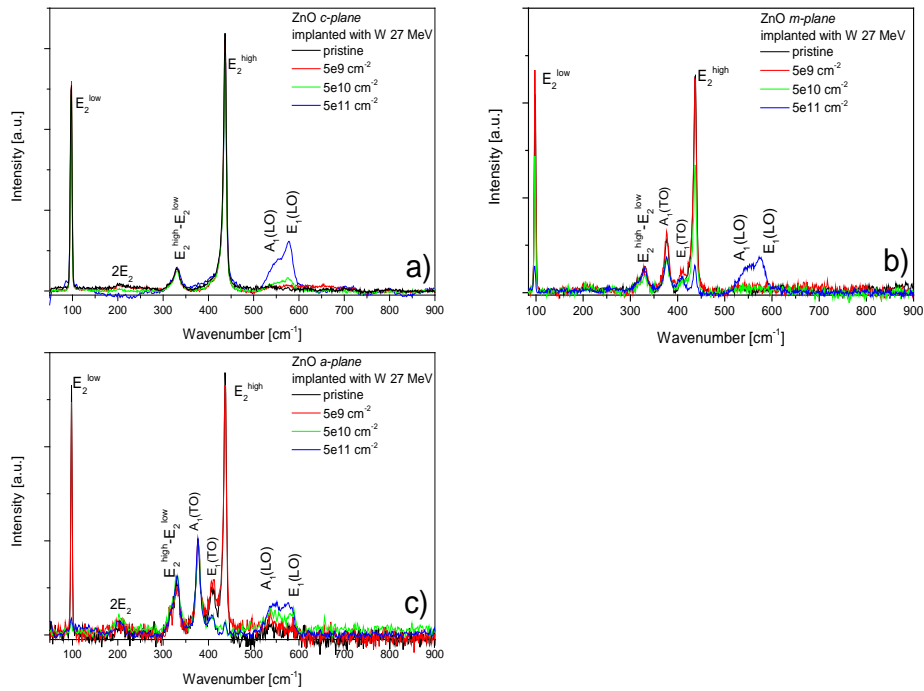


Figure 3 - Raman spectra of irradiated samples with W ions with energy 27 MeV for a) *c-plane*, b) *m-plane* and c) *a-plane* ZnO

5.2. Surface morphology

The $3 \times 3 \mu\text{m}^2$ AFM scans were used to estimate the irradiation effect on the surface morphology of ZnO crystals and on the surface roughness. The surface roughness is determined with a root means square (RMS) of surface height distribution.

Figure 4a-d shows AFM images of the pristine as well as the irradiated *c-plane* ZnO and Figure 5a-d shows AFM images of the pristine as well as the irradiated *a-plane* ZnO. The irradiation effect is clearly visible. The pristine sample shows a low surface roughness 0.74 nm without any significant objects, only the slight porosity is observed being evidenced already before on the hydrothermally grown ZnO crystalline facets [34]. The W-ion irradiation does not lead to a rapid change in surface roughness since for the lowest irradiation fluence the RMS parameter slightly increases to the value 1.38 nm. For the highest irradiation fluence, RMS parameter is estimated as 5.84 nm. However, the W-ion irradiation shows impact on the surface morphology and causes formation of grains. The fluence $5 \times 10^9 \text{ cm}^{-2}$ should correspond to the single ion implantation regime where the damage caused by particular ions is separated. The single ion impact in *c-plane* ZnO shown at Figure 4b indicates low density of present grains which seems to be separated from each other. Further increase of the irradiation fluence leads to enhancement of grains density and its overlapping. For the highest fluence $5 \times 10^{11} \text{ cm}^{-2}$ shown at the Figure 4d (overlapping ion implantation regime), it seems that density of present grains is high enough to create nearly continuous rough layer with objects reaching heights of several tens of nm. The distribution of grain size determined by grain diameter is broadening with irradiation fluence as it is seen on the Figure 4 and shows higher portion of grains with larger diameter.

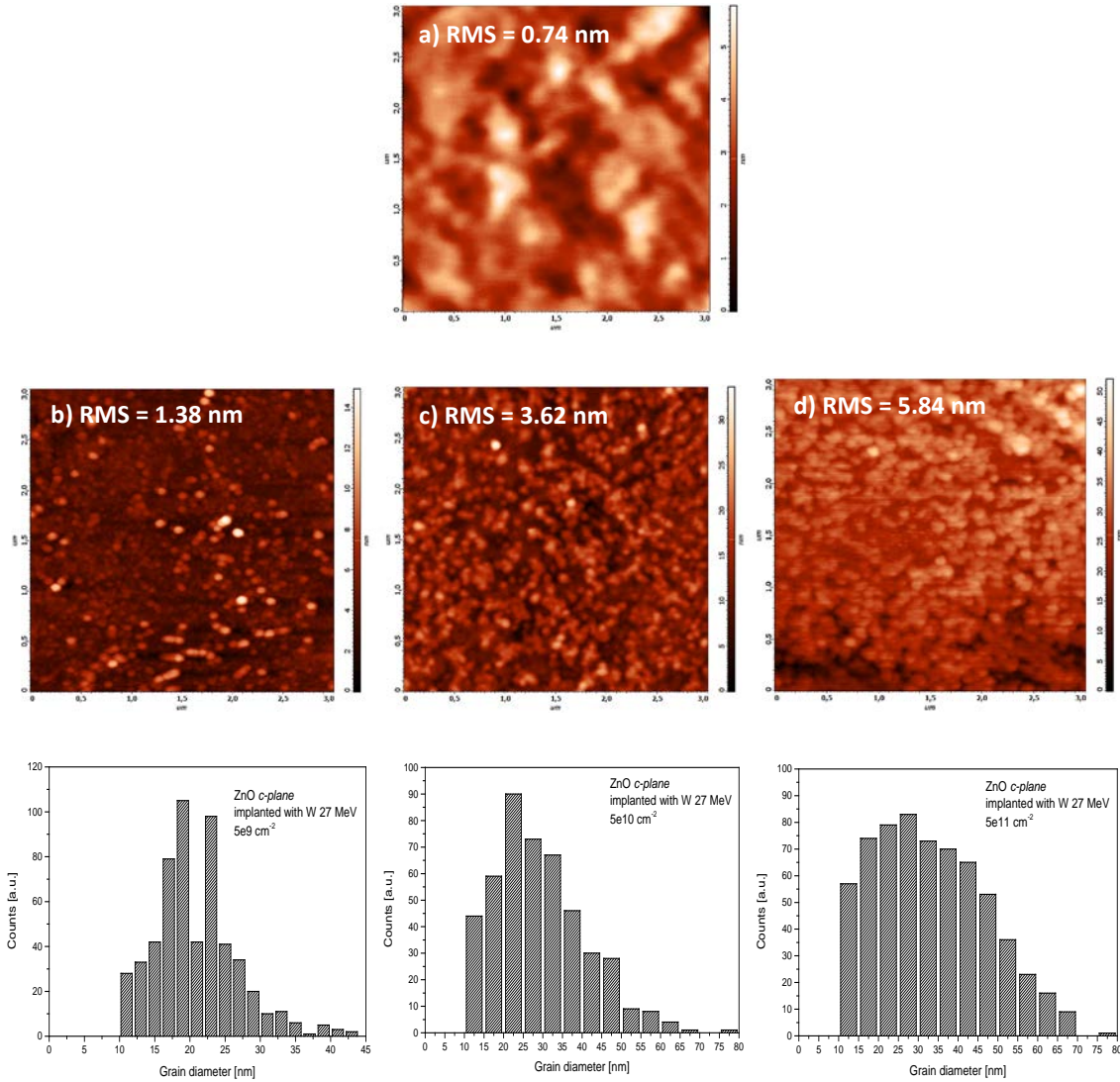


Figure 4 – Comparison of AFM 2D images and corresponding grain size distributions for *c-plane* ZnO a) pristine and irradiated with fluences b) $5 \times 10^9 \text{ cm}^{-2}$, c) $5 \times 10^{10} \text{ cm}^{-2}$ and d) $5 \times 10^{11} \text{ cm}^{-2}$.

The *a-plane* ZnO roughness and surface morphology are similar to *c-plane* ZnO. However, evolution of morphology change is slower than in case of *c-plane* ZnO. The formation of separated grains starts with fluence $5 \times 10^{10} \text{ cm}^{-2}$ as is seen on the Figure 5b and even for the highest fluence grains do not create completely compact layer. The RMS parameter seems to be increased less progressively in comparison to *c-plane* ZnO, nevertheless the RMS values are comparable, especially for the highest fluence. Looking at the distribution of grain size, the *a-plane* ZnO irradiated with fluence $5 \times 10^{10} \text{ cm}^{-2}$ forms mostly small grains. The higher irradiation fluence leads to the broadening and to the shift of grain size distribution to the higher values for *a-plane* ZnO crystals.

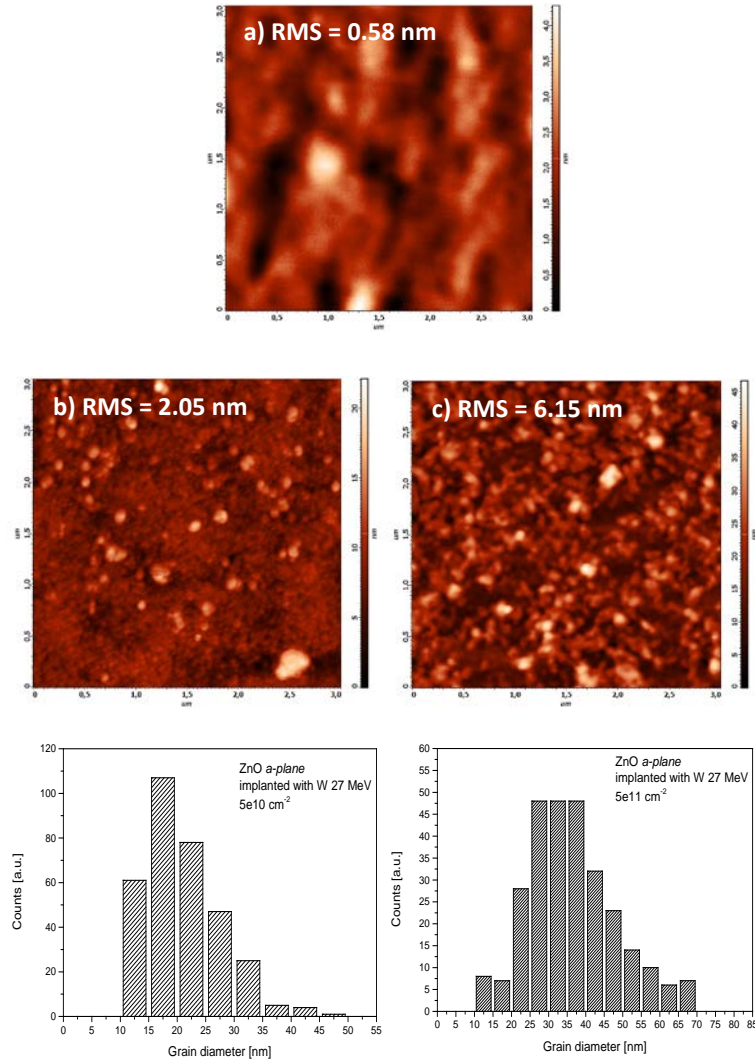


Figure 5 - Comparison of AFM 2D images and corresponding grain size distributions for *a-plane* ZnO a) pristine, b) $5 \times 10^{10} \text{ cm}^{-2}$ and c) $5 \times 10^{11} \text{ cm}^{-2}$.

The non-polar *m-plane* ZnO surfaces, see at Figure 6a-c, exhibit highest level of surface modification. Even the surface roughness of pristine sample ($\text{RMS} = 1.82 \text{ nm}$) is higher than in case of *c-plane* and *a-plane* ZnO. The irradiation leads to rapid increase in surface roughness with irradiation fluence and for the highest fluence it reaches $\text{RMS} = 10.07 \text{ nm}$. From the AFM results it seems that *m-plane* ZnO is much more modified than both previous crystallographic orientations. Simultaneously, the surface morphology is different for *m-plane* ZnO facet and for the lower fluences represent more sponge-like networks with nuclei of emerging grains (Figure 6b) which is converted to the fully grainy pattern for the sample irradiated with the highest fluence (Figure 6c). This *m-plane* ZnO morphology is much progressively modified by ion bombardment as was already observed in [26]. The specific *m-plane* structure can be result of aggregation of smaller defects supported by energy transfer from highly energetic W ions and therefore it can form sponge-like network or grain clusters.

The *m-plane* ZnO shows the widest grain size distribution for lower as well as higher irradiation fluence with grain diameters reaching 100 nm.

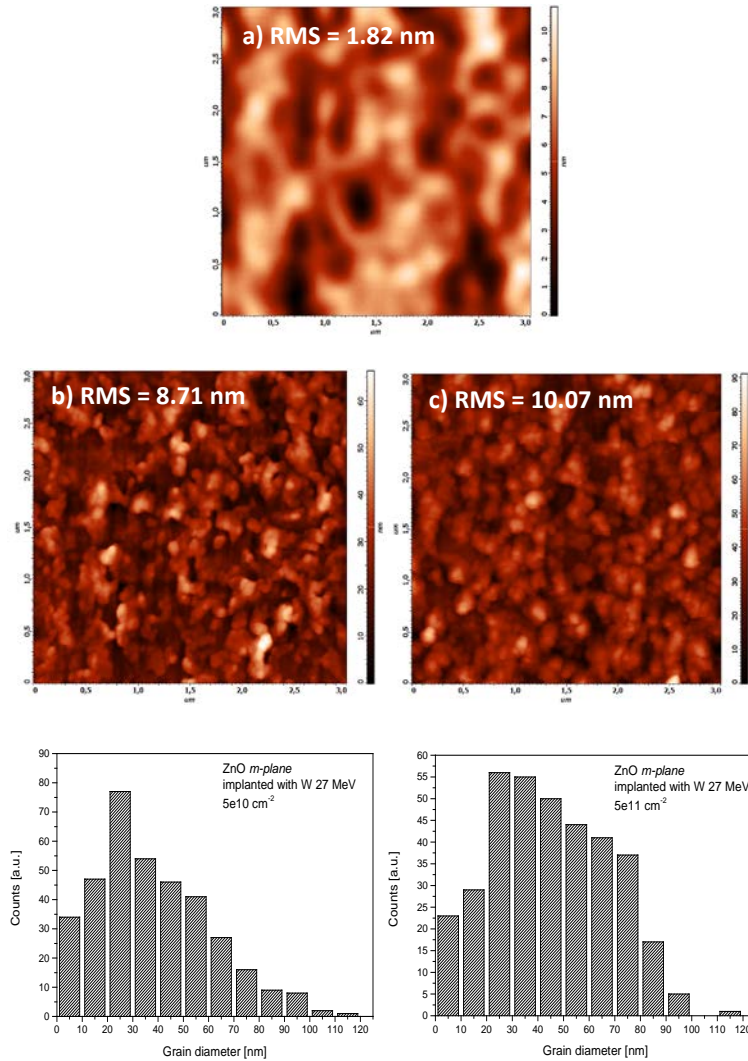


Figure 6 – Comparison of AFM 2D images and corresponding grain size distributions for *m-plane* ZnO a) pristine, b) $5 \times 10^{10} \text{ cm}^{-2}$ and c) $5 \times 10^{11} \text{ cm}^{-2}$.

5.3. Optical characterization

The spectroscopic ellipsometry (SE) was used to follow the surface roughness and mainly the optical constants, such as index of refraction n and extinction coefficient k , modifications before and after the W-ion irradiation. Wurtzite ZnO is a uniaxial optically anisotropic material which optical properties are described by ordinary and extraordinary complex refractive indices ($n-ik$). [35] However, evaluation of ordinary and extraordinary optical constants for *c-plane* ZnO crystals is not an easy task due to the orientation of the optical axis that is perpendicular with respect to the *c-plane* [36]. Therefore, the SE results for *c-plane* ZnO show only effective values of n and k which are close to the ordinary constants (see Figure 7a). For *a-plane* ZnO (Figure 7b) and *m-plane* ZnO both the ordinary as well as the

extraordinary, n and k values were evaluated. The SE spectra for *m-plane* ZnO are nearly identical to the results for *a-plane* and are not presented in the article.

Penetration depth of light in ZnO depends on photon energy, thus for photon energies below ZnO optical band gap the material is optically transparent and light can penetrate into the depth equal to several μm . In this transparent region the SE spectra (recorded in reflected beam) are nearly unaffected by W-ion irradiation process and are comparable with pristine samples. The W-ion accumulation depth is estimated to be around 3.8 μm and the used irradiation fluences should correspond to the W concentration significantly below 1 at. %, therefore we didn't expect that W enriched layer contribute to the optical properties modification in transparent region. However, the SE spectra of the W-ion irradiated ZnO show a clear change of n (Figure 7a,c) as well as k (Figure 7b,d) coefficients in the absorption region of energies above the band gap. All SE spectra of the pristine samples exhibit sharp exciton peak at about 3.3 eV that is typical for ZnO. It is in fact the A, B exciton doublet, which is not resolved at room temperature measurement and also C exciton or exciton-phonon complexes (EPC) located on the higher energy shoulder of A, B doublet peak (see indication in Figure 7). [35] These features were much less visible in the SE spectra of the irradiated samples. The exciton peaks were blurred and slightly lowered after the W-ion irradiation. This was visible mainly for the extinction coefficient of irradiated *c-plane* crystal, where the slight decrease of n and k is visible for energies above 3.25 eV as it is shown in Figure 7a. The lowering of the optical constants and the higher absorption in ZnO was observed in Redondo-Cubero et al. [22] as a consequence of 20 keV Ar-ion implantation induced damage and partial amorphization. As it was shown in literature, amorphous and polycrystalline ZnO exhibits lower refractive index than single crystalline ZnO [37–39], so the decrease of optical constants can be ascribed to a dislocation of lattice atoms in ZnO matrix caused by ion irradiation. Similar effect was observed for doped silicon (especially for excitonic E_1 peak), where the doping leads to lowering and smoothening of optical n and k functions [40] as well as for polycrystalline and microcrystalline silicon due to amorphization [41]. The surface morphology modification, observed with AFM, also contributes to the ellipsometric spectra. This is most remarkable above the band gap since the penetration depth for these photon energies is just few nm.

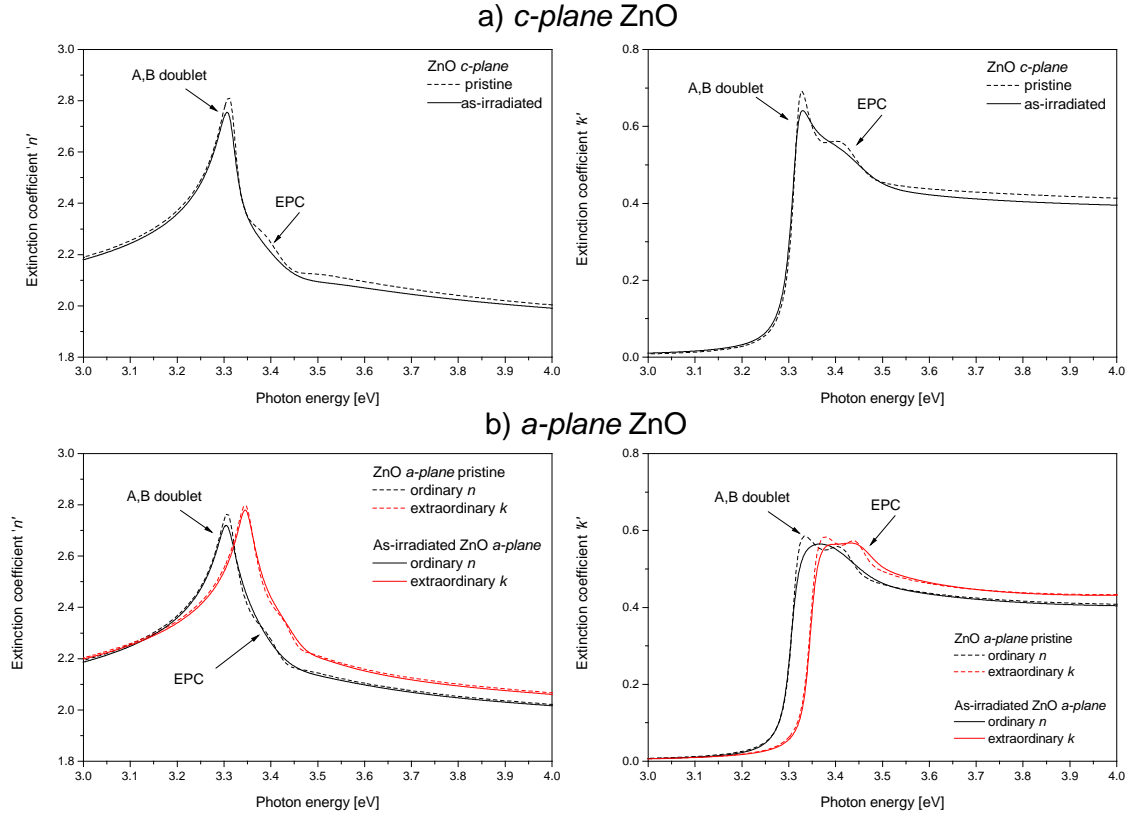


Figure 7 – Refraction (n) and extinction (k) coefficients determined from ellipsometric measurement for pristine and ZnO irradiated with highest fluence $5 \times 10^{11} \text{ cm}^{-2}$ of a) c -plane and b) a -plane ZnO crystals irradiated by 27 MeV W ions

Therefore, the obtained SE data were fitted against a sample model incorporating also surface roughness by means of Bruggeman effective medium approximation [42]. The SE extracted values of surface roughness show relatively smooth surface of the pristine samples with a roughness from 2.2 nm (m -plane) up to 3.7 nm (c -plane). The W-ion irradiation leads to the increase of the surface roughness and the SE extracted roughness values are summarized in Table 2 and compared to the AFM determined RMS parameters. The smallest surface roughness change was observed for m -plane ZnO, where the roughness increases to the value 3.4 nm. In case of c -plane and a -plane ZnO the roughness exceeds 6.0 nm after irradiation. The surface roughness determined from ellipsometry is not identical to that determined from AFM, but it follows the same trend of increasing roughness after irradiation. The c -plane and a -plane ZnO show similar surface roughness which is in agreement of both SE and AFM measurement. The m -plane ZnO roughness determined by SE seems to be the less affected by the W-ion irradiation, which is contrary to the AFM measurement. Nevertheless, it should be emphasized that the roughness determined by SE analysis is realized from the significantly larger area (beam size diameter of about 6 mm) compared to AFM, where the scans are $3 \mu\text{m} \times 3 \mu\text{m}$. The SE is not sensitive to isolated defects and it may ignore some higher objects on

the surface, thus the roughness can be lower in comparison to AFM but it can also indicate that *m-plane* modification is not completely homogenous for the whole sample surface.

Table 2 - Surface roughness determined by spectroscopic ellipsometry (SE) and by AFM measurement

| Sample and method | ZnO <i>c-plane</i> roughness [nm] | ZnO <i>m-plane</i> roughness [nm] | ZnO <i>a-plane</i> roughness [nm] |
|--|--------------------------------------|--------------------------------------|--------------------------------------|
| Pristine (SE) | 3.7 | 2.2 | 3.5 |
| $5 \times 10^{11} \text{ cm}^{-2}$ (SE) | 6.3 | 3.4 | 6.0 |
| Pristine (AFM) | 0.7 | 1.8 | 0.6 |
| $5 \times 10^{11} \text{ cm}^{-2}$ (AFM) | 5.8 | 10.1 | 6.2 |

The Figure 8 presents photoluminescence (PL) spectra of the pristine and the irradiated samples. The PL spectra of crystalline ZnO show two bands around 376 nm and 540 nm. The sharp peak at 376 nm is assigned to the exciton recombination and it is referred as a Near-band edge (NBE) peak. The origin of a green luminescence (GL) represented by broad deep-level emission (DLE) peak at 540 nm is not completely understood yet, but it is mostly associated with native point defects in crystal structure mainly to the oxygen (V_O), zinc (V_{Zn}) vacancies or zinc antisites (O_{Zn}). [43]

All crystallographic ZnO facets show similar decreasing trend of both NBE and DLE peaks. This can be related to the stress field generated by ion irradiation resulting in non-radiative process. [43] The irradiation with low fluence $5 \times 10^9 \text{ cm}^{-2}$ leads to the small changes in the intensity of PL spectra. Moreover, the PL results for *a-plane* ZnO exhibit only small reduction of DLE peak and the NBE signal copy intensity obtained from the pristine sample. After the W-ion irradiation with the higher fluences, the PL intensities rapidly drop down for all facets and in case of the *m-plane* ZnO, the irradiation with fluence $5 \times 10^{11} \text{ cm}^{-2}$ results nearly in a complete disappearance of NBE peak. The shift of PL intensity maxima was not observed after irradiation with W ions.

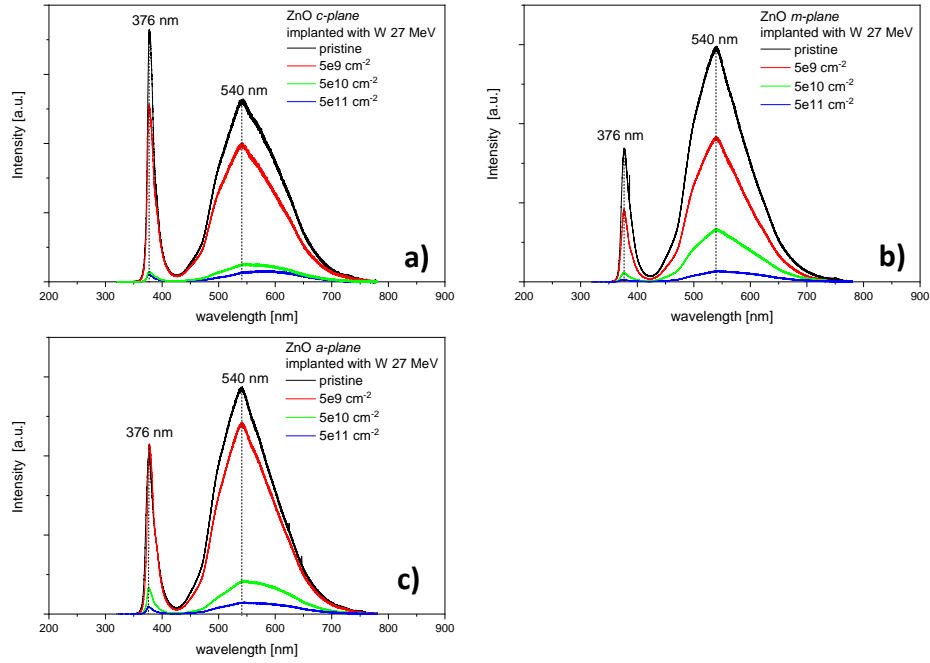


Figure 8 - PL spectra for ZnO implanted with W ions with energy 27 MeV for a) c-plane, b) m-plane, c) a-plane

Focusing on the NBE and DLE peak decline, the NBE/DLE intensity ratios are summarized in Table 3. The rapid reduction of both NBE and DLE peaks follows the irradiation with fluence $5 \times 10^{10} \text{ cm}^{-2}$ and their intensity decreases under 22 % for all ZnO orientations. The most progressive decline is observed for *m-plane* samples, where the NBE in the sample irradiated with fluence $5 \times 10^9 \text{ cm}^{-2}$ drops nearly about 50 % compared to the pristine sample. Further the decrease to the 1 % of the original intensity for the highest W-ion irradiation fluence was observed. ZnO *a-plane* samples are the least affected by the W-ion irradiation. The intensity of NBE peak does not exhibit any difference between intensity of the pristine and the irradiated *a-plane* ZnO at the lowest fluence. The DLE peak decreases about 16 %. Both NBE and DLE peaks are reduced for the samples irradiated with the higher W-ion fluence, moreover, the DLE peak of *a-plane* ZnO is reduced more progressively than NBE. In contrast to *a-plane*, DLE peak of *c-plane* and *m-plane* crystals decreases less progressively than NBE. The above mentioned phenomena can be correlated to the distinct radiation damage in various ZnO facets caused by the energetic W-ion irradiation.

Table 3 – Comparison of NBE/DLE intensities in contrast to its original (pristine) state

| Sample | ZnO <i>c-plane</i> NBE/DLE intensity [%] | ZnO <i>m-plane</i> NBE/DLE intensity [%] | ZnO <i>a-plane</i> NBE/DLE intensity [%] |
|----------|--|--|--|
| Pristine | 100/100 | 100/100 | 100/100 |

| | | | |
|------------------------------------|-------|-------|--------|
| $5 \times 10^9 \text{ cm}^{-2}$ | 70/74 | 54/61 | 100/84 |
| $5 \times 10^{10} \text{ cm}^{-2}$ | 4/10 | 7/22 | 16/14 |
| $5 \times 10^{11} \text{ cm}^{-2}$ | 3/5 | 1/4 | 5/5 |

6. Discussion

Polar *c-plane* and non-polar *a-plane* and *m-plane* ZnO crystals have been irradiated by highly energetic W ions to study crystal damage evolution in the sub-surface layer as well as on the surface. According to the SRIM calculations, the electron stopping prevails in a sub-surface region and steeply decreases with ion penetration depth. It defines the depth of interest up to 1 μm , where the ZnO modification has been preferentially caused by ionization processes. The structural changes have been analysed by RBS-C and Raman spectroscopy to distinguish between various defect types. Back-scattered ion de-channeling in RBS-C analysis is sensitive to specific defects connected to the disorder in Zn sub-lattice such as deformation of the atomic rows parallel to the incoming beam e.g. prismatic loops, Zn interstitial atoms and point defects, highly distorted region as atomic clusters, but it is not so sensitive to defects connected to dislocation loops in basal planes, O displacements and O sub-lattice disorder. From RBS-C measurement, Zn sub-lattice of *a-plane* ZnO seems to be less affected by the W-ion irradiation and the yield of backscattered ions significantly increases only after ion irradiation with the highest fluence in comparison to the *c-plane* and mainly *m-plane* ZnO, in the latter one the highest normalized yield has been evidenced. However, the Raman spectra of irradiated *a-plane* ZnO show significant change exhibited mainly by rapid reduction of E_2^{high} and appearance of $A_1(\text{LO})$ and $E_1(\text{LO})$ Raman modes. The Raman spectroscopy reflects molecular vibration states and thus it is sensitive also to the oxygen defects, in contrast to RBS-C. In particular, the E_2^{high} peak reduction is related to the growing disorder in O sub-lattice. Further, the appearance of polar modes $A_1(\text{LO})$ and $E_1(\text{LO})$ is mostly attributed to presence of V_{O} . [32] Therefore, we can assume that ion irradiation causes reorganization of O sub-lattice accompanied by increase of V_{O} in *a-plane* ZnO. In case of *c-plane* samples, the irradiation does not cause significant increase in intensity of E_2^{high} peak and the polar modes $A_1(\text{LO})$ and $E_1(\text{LO})$ appeared only after irradiation with the highest fluence. This can indicate better resistance of O sub-lattice of *c-plane* ZnO due to radiation damage as was observed also in [26]. The radiation defects mostly result in creation of Frenkel's pairs, interstitial and vacancy pairs of lattice atoms dislocated from its original position as a result of elastic collisions. Creation of these defects is linked to the displacement energies of particular

elements. In Cowen and El-Genk [44], simulations of threshold energies for Frenkel's pairs creations in metal oxides predicted crystallographic orientation dependency of displacement energies for oxygen as well as metal atoms and so distinguished defect creation in particular crystallographic planes. We can assume that highly energetic ion irradiation and so the electronic stopping forces can cause similar defect resulting from higher thermal movement of the lattice atoms induced by energy of thermal spike. In contrast to the both non-polar facets, the damage in O sub-lattice in polar *c-plane* ZnO can be lowered due to lattice arrangement since O lattice atoms are shadowed by Zn during the ion irradiation experiment.

The surface morphology analysed by AFM shows distinctive surface morphology of particular ZnO orientations. The *c-plane* as well as *a-plane* ZnO surfaces tend to form small grains on the surface after irradiation. The density of these grains increases with the W-ion irradiation fluence and can form the continuous layer. The irradiated *m-plane* ZnO surfaces show dissimilar morphology and for the lower irradiation fluences create sponge-like network which could be related to the aggregation of surface defects due to higher surface mobility supported by irradiation process. The highest W-ion fluence cause formation of surface grains which can be attributed to the surface self-organisation caused by increased bombardment with highly energetic ions and therefore to the higher energy transfer from the W ions to the surface atoms. The similar transformation from sponge-like network to the surface grains was showed previously for germanium irradiated by Bi ions [45] where the self-organisation was supported mainly by the increase of substrate temperature during the ion bombardment up to 700 K (427 °C). The distinctive surface morphology of polar and non-polar ZnO was observed even in our previous experiment with ZnO irradiation with Au 30 MeV [26] where non-polar *m-plane* ZnO exposed by energetic Au ions exhibited formation of huge mounds in contrast to small hillocks created on the *c-plane* and *a-plane* ZnO surfaces. However, the sponge-like stage of *m-plane* facet was not observed in this experiment.

The surface roughness determined by RMS parameter tends to gradually increase with ion irradiation fluence for all studied facets but several differences were observed. The *a-plane* ZnO roughness increase slower than the roughness of *c-plane* ZnO, nevertheless their values are comparable. This was observed also with SE measurement. The RMS parameter of *m-plane* ZnO exhibits the highest roughness which is contra SE measurement. The difference may be caused by worse homogeneity of *m-plane* nanostructured surfaces.

The W ion irradiated samples show decrease of the total luminescence which is connected to the creation of non-radiative processes and it is accompanied with reduction both NBE and DLE peaks in PL spectra. PL intensities decline gradually with irradiation fluence and both NBE as well as DLE. Generally, non-polar *a-plane* facet seems to be less affected by irradiation and reduction of peak intensities is lower in comparison to the other studied facets. This was observed also in [23,26]. Moreover, the DLE peak decrease faster than NBE in case of *a-plane* ZnO samples. The origin of green luminescence represented by DLE peak is still not completely understood and is mostly attributed to V_O , V_{Zn} and O_{Zn} . Nevertheless, the previously reported calculations show that V_{Zn} is a deep acceptor with a low formation energy and therefore V_{Zn} can be the main source of green luminescence.[46] This was confirmed in [47], where the combination of Positron Annihilation Spectroscopy (PAS) with PL measurement was used to find the correlation between green luminescence peak position and particular ZnO defects and assigned the peak at the 540 nm (2.3 eV) to the higher density of V_{Zn} . Therefore, it can be assumed that higher PL and mainly DLE peak intensity of irradiated *a-plane* ZnO in contrast to *c-plane* and *m-plane* ZnO is related to the better radiation resistance of Zn sub-lattice confirmed by RBS/C. The *m-plane* facet shows the highest decrease of NBE and DLE peak intensity and it further represents the highest Zn sub-lattice disorder in RBS-C. In our previous experiment presented in [26], the Au-ion irradiation caused strong suppression of NBE as well as DLE peaks mainly in *m-plane* ZnO as was observed also after W-ion irradiation. Moreover, the Au-ion irradiated ZnO exhibited shift of DLE peak towards higher wavelength. This shift is mostly connected to the presence of extended defects and V_{Zn} clusters [48]. The presence of defect clusters in Au irradiated ZnO was confirmed also by PAS analysis. This shift has not been observed after irradiation with W ions. This can indicate, that crystal damage caused by W-ion irradiation consist mainly from point defects.

All facets show similar trend of slight decrease of optical constants in optical band gap region and blurring of features belonging to particular excitons after ion irradiation. However, small difference has been seen in the photon energies above band gap. Polar *c-plane* ZnO shows a decrease in a whole absorption range in contrast to non-polar *a-plane* and *m-plane* facets, where the change is observed only in band gap region and for higher photon energies n and k functions of irradiated samples copy function of pristine sample. The decrease in optical coefficients and change of their functions may be result of damage caused by ion irradiation as was observed by group of Redondo-Cubero [22] combined with change in surface

morphology. As was shown on AFM figures, the ion irradiation causes creation of small grains on the ZnO surface which could be randomly oriented. This can exhibit the similar effect as presence of polycrystalline layer and so change in functions of optical constants as it was observed in case of silicon in [49].

7. Conclusion

The aim of this experiment was study of surface nanostructures of various ZnO facets prepared via high energy ion irradiation with energy. The polar *c-plane* and non-polar *a-plane* and *m-plane* facets were irradiated with 27 MeV W ions with fluences varying from $5 \times 10^9 \text{ cm}^{-2}$ to $5 \times 10^{11} \text{ cm}^{-2}$ to see distinctive effect of single ion impact and overlapping ion impact.

Particular crystallographic facets exhibit distinctive defect character caused by ion irradiation. The RBS-C showed strong radiation resistance of Zn sub-lattice of *a-plane* ZnO, nevertheless the rapid change in Raman spectra point out to the high O sub-lattice disorder and presence of V_O . Defect character plays an important role as well in optical properties of ZnO. Despite the significant presence of O defects, the photoluminescence peaks NBE and DLE were the least reduced after irradiation of *a-plane* ZnO. On the contrary, the irradiation of *m-plane* ZnO promotes the strongest inhibition of photoluminescence resulting from the highest accumulation of Zn defects as was proved by RBS-C.

The AFM measurement revealed specific nanostructuring of particular facets. The *c-plane* and *a-plane* ZnO formed small separated grains on the surface after exposure with low irradiation fluences with single ion impact and tended to cumulate with increasing ion impact. The *m-plane* ZnO exhibited two stages of surface modification starting with sponge-like network for lower fluences and conversion to grainy surface for the highest fluence. Simultaneously, the *m-plane* ZnO showed the highest roughness measured with AFM in contrast to SE analysis, where the roughness was the lowest from all studied facets. This discrepancy may be caused by worse homogeneity of *m-plane* nanostructures and it will probably need more attention to completely understand to formation mechanism of surface nanostructures on the non-polar ZnO facets.

8. Acknowledgements

The research has been carried out at the CANAM (Centre of Accelerators and Nuclear Analytical Methods) infrastructure LM 2015056. This publication has been supported by the University of J. E. Purkyne project UJEP-SGS-2021-53-002-2.

The authors acknowledge the assistance provided by the Research Infrastructure NanoEnviCz, supported by the Ministry of Education, Youth and Sports of the Czech Republic under Project No. LM2018124 and LM2018103.

9. References

- [1] G.C. Vásquez, K.M. Johansen, A. Galeckas, L. Vines, B.G. Svensson, Optical signatures of single ion tracks in ZnO, *Nanoscale Adv.* 2 (2020) 724–733. <https://doi.org/10.1039/C9NA00677J>.
- [2] M. Jubera, A. García-Cabañes, J. Olivares, A. Alcazar, M. Carrascosa, Particle trapping and structuring on the surface of LiNbO₃:Fe optical waveguides using photovoltaic fields, *Opt. Lett.* 39 (2014) 649. <https://doi.org/10.1364/OL.39.000649>.
- [3] S. Wolf, J. Rensberg, A. Johannes, R. Thomae, F. Smit, R. Neveling, M. Moodley, T. Bierschenk, M. Rodriguez, B. Afra, S.B. Hasan, C. Rockstuhl, M. Ridgway, K. Bharuth-Ram, C. Ronning, Shape manipulation of ion irradiated Ag nanoparticles embedded in lithium niobate, *Nanotechnology*. 27 (2016) 145202. <https://doi.org/10.1088/0957-4484/27/14/145202>.
- [4] M. Sall, I. Monnet, F. Moisy, C. Grygiel, S. Jublot-Leclerc, S. Della-Negra, M. Toulemonde, E. Balanzat, Track formation in III-N semiconductors irradiated by swift heavy ions and fullerene and re-evaluation of the inelastic thermal spike model, *J. Mater. Sci.* 50 (2015) 5214–5227. <https://doi.org/10.1007/s10853-015-9069-y>.
- [5] A. Colder, B. Canut, M. Levalois, P. Marie, X. Portier, S.M.M. Ramos, Latent track formation in GaAs irradiated with 20, 30, and 40 MeV fullerenes, *J. Appl. Phys.* 91 (2002) 5853–5857. <https://doi.org/10.1063/1.1467962>.
- [6] A. Kozlovskiy, K. Dukenbayev, I. Ivanov, S. Kozin, V. Aleksandrenko, A. Kurakhmedov, E. Sambaev, I. Kenzhina, D. Tosi, V. Loginov, M. Zdorovets, Investigation of the influence of irradiation with Fe⁺⁷ ions on structural properties of AlN ceramics, *Mater. Res. Express*. 5 (2018) 065502. <https://doi.org/10.1088/2053-1591/aac7ba>.
- [7] J.H. O’Connell, G. Aralbayeva, V.A. Skuratov, M. Saifulin, A. Janse van Vuuren, A. Akilbekov, M. Zdorovets, Temperature dependence of swift heavy ion irradiation induced hillocks in TiO₂, *Mater. Res. Express*. 5 (2018) 055015. <https://doi.org/10.1088/2053-1591/aac0ce>.
- [8] M. Karlušić, M. Jakšić, H. Lebius, B. Ban-d’Etat, R.A. Wilhelm, R. Heller, M. Schleberger, Swift heavy ion track formation in SrTiO₃ and TiO₂ under random, channeling and near-channeling conditions, *J. Phys. Appl. Phys.* 50 (2017) 205302. <https://doi.org/10.1088/1361-6463/aa678c>.
- [9] A. Redondo-Cubero, K. Lorenz, F.J. Palomares, A. Muñoz, M. Castro, J. Muñoz-García, R. Cuerno, L. Vázquez, Concurrent segregation and erosion effects in medium-energy iron beam patterning of silicon surfaces, *J. Phys. Condens. Matter*. 30 (2018) 274001. <https://doi.org/10.1088/1361-648X/aac79a>.
- [10] J.-H. Kim, S.M. Yoon, S. Jo, J. Seo, J.-S. Kim, Nanopatterning by ion beam sputtering in unconventional formats, *J. Phys. Condens. Matter*. 30 (2018) 274004. <https://doi.org/10.1088/1361-648X/aac7d7>.
- [11] S. Facsko, Formation of Ordered Nanoscale Semiconductor Dots by Ion Sputtering, *Science*. 285 (1999) 1551–1553. <https://doi.org/10.1126/science.285.5433.1551>.
- [12] L.Q. Zhang, C.H. Zhang, J.J. Li, Y.C. Meng, Y.T. Yang, Y. Song, Z.N. Ding, T.X. Yan, Damage to epitaxial GaN layer on Al₂O₃ by 290-MeV 238U³²⁺ ions irradiation, *Sci. Rep.* 8 (2018) 4121. <https://doi.org/10.1038/s41598-018-22321-w>.
- [13] R. Dell’Anna, E. Iacob, M. Barozzi, L. Vanzetti, R. Hübner, R. Böttger, D. Giubertoni, G. Pepponi, The role of incidence angle in the morphology evolution of Ge surfaces irradiated by medium-energy Au ions, *J. Phys. Condens. Matter*. 30 (2018) 324001. <https://doi.org/10.1088/1361-648X/aacf5f>.
- [14] A. Camellini, A. Mazzanti, C. Mennucci, C. Martella, A. Lamperti, A. Molle, F. Buatier de Mongeot, G. Della Valle, M. Zavelani-Rossi, Evidence of Plasmon Enhanced Charge Transfer in

- Large-Area Hybrid Au–MoS₂ Metasurface, *Adv. Opt. Mater.* 8 (2020) 2000653.
<https://doi.org/10.1002/adom.202000653>.
- [15] Z.-Y. Zhao, Z.-Q. Song, W.-Z. Shi, Q.-Z. Zhao, Optical absorption and photocurrent enhancement in semi-insulating gallium arsenide by femtosecond laser pulse surface microstructuring, *Opt. Express*. 22 (2014) 11654. <https://doi.org/10.1364/OE.22.011654>.
- [16] S. Achilli, N.H. Le, G. Fratesi, N. Manini, G. Onida, M. Turchetti, G. Ferrari, T. Shinada, T. Tanii, E. Prati, Position-Controlled Functionalization of Vacancies in Silicon by Single-Ion Implanted Germanium Atoms, *Adv. Funct. Mater.* (2021) 2011175.
<https://doi.org/10.1002/adfm.202011175>.
- [17] Ž. Pastuović, R. Siegele, I. Capan, T. Brodar, S. Sato, T. Ohshima, Deep level defects in 4H-SiC introduced by ion implantation: the role of single ion regime, *J. Phys. Condens. Matter*. 29 (2017) 475701. <https://doi.org/10.1088/1361-648X/aa908c>.
- [18] G.C. Vásquez, Optical signatures of single ion tracks in ZnO, (2020) 10.
- [19] V. Pelenovich, X. Zeng, R. Rakhimov, W. Zuo, C. Tian, D. Fu, B. Yang, Decoration of ZnO needles with nanoripples using gas cluster ion bombardment, *Mater. Lett.* 264 (2020) 127356.
<https://doi.org/10.1016/j.matlet.2020.127356>.
- [20] E. de Prado, C. Florian, B. Sotillo, J. Siegel, J. Solis, P. Fernández, Optical spectroscopy study of nano- and microstructures fabricated by femtosecond laser pulses on ZnO based systems, *CrystEngComm*. 20 (2018) 2952–2960. <https://doi.org/10.1039/C8CE00436F>.
- [21] V. Kondkar, D. Rukade, D. Kanjilal, V. Bhattacharyya, Controlled morphological modifications of ZnO thin films by ion irradiation, *Mater. Res. Express*. 4 (2017) 116402.
<https://doi.org/10.1088/2053-1591/aa9580>.
- [22] Redondo-Cubero, Vázquez, Jalabert, Lorenz, Sedrine, Modelling of Optical Damage in Nanorippled ZnO Produced by Ion Irradiation, *Crystals*. 9 (2019) 453.
<https://doi.org/10.3390/cryst9090453>.
- [23] A. Macková, P. Malinský, A. Jagerová, R. Mikšová, P. Nekvindová, J. Cajzl, R. Böttger, S. Akhmadaliev, Au incorporation into various ZnO crystallographic cuts realised by ion implantation – ZnO damage characterization, *Vacuum*. 169 (2019) 108892.
<https://doi.org/10.1016/j.vacuum.2019.108892>.
- [24] A. Jagerová, P. Malinský, R. Mikšová, P. Nekvindová, J. Cajzl, P. Ryšánek, A. Macková, High energy Au⁺ ion implantation of polar and nonpolar ZnO-Structure modification and optical properties, *Surf. Interface Anal.* (2020). <https://doi.org/10.1002/sia.6789>.
- [25] A. Macková, A. Jagerová, P. Malinský, M. Cutroneo, J. Flaks, P. Nekvindová, A. Michalcová, V. Holý, T. Košutová, Nanostructures in various Au ion-implanted ZnO facets modified using energetic O ions, *Phys. Chem. Chem. Phys.* 22 (2020) 23563–23573.
<https://doi.org/10.1039/D0CP04119J>.
- [26] A. Jagerová, P. Malinský, R. Mikšová, O. Lalik, M. Cutroneo, O. Romanenko, K. Szökölóvá, Z. Sofer, P. Slepíčka, J. Čížek, A. Macková, Modification of structure and surface morphology in various ZnO facets via low fluence gold swift heavy ion irradiation, *Surf. Interface Anal.* (2020) sia.6904. <https://doi.org/10.1002/sia.6904>.
- [27] J.F. Ziegler, M.D. Ziegler, J.P. Biersack, SRIM – The stopping and range of ions in matter (2010), *Nucl. Instrum. Methods Phys. Res. Sect. B Beam Interact. Mater. At.* 268 (2010) 1818–1823.
<https://doi.org/10.1016/j.nimb.2010.02.091>.
- [28] G. Jayalakshmi, K. Saravanan, S. Balakumar, T. Balasubramanian, Swift heavy ion induced modifications in structural, optical & magnetic properties of pure and V doped ZnO films, *Vacuum*. 95 (2013) 66–70. <https://doi.org/10.1016/j.vacuum.2013.02.014>.
- [29] C. Tanguy, Optical Dispersion by Wannier Excitons, *Phys. Rev. Lett.* 75 (1995) 4090–4093.
<https://doi.org/10.1103/PhysRevLett.75.4090>.
- [30] C. Boemare, T. Monteiro, M.J. Soares, J.G. Guilherme, E. Alves, Photoluminescence studies in ZnO samples, *Phys. B Condens. Matter*. 308–310 (2001) 985–988.
[https://doi.org/10.1016/S0921-4526\(01\)00854-7](https://doi.org/10.1016/S0921-4526(01)00854-7).

- [31] T. Kaida, K. Kamioka, T. Ida, K. Kuriyama, K. Kushida, A. Kinomura, Rutherford backscattering and nuclear reaction analyses of hydrogen ion-implanted ZnO bulk single crystals, *Nucl. Instrum. Methods Phys. Res. Sect. B Beam Interact. Mater. At.* 332 (2014) 15–18. <https://doi.org/10.1016/j.nimb.2014.02.020>.
- [32] Y. Song, S. Zhang, C. Zhang, Y. Yang, K. Lv, Raman Spectra and Microstructure of Zinc Oxide irradiated with Swift Heavy Ion, *Crystals*. 9 (2019) 395. <https://doi.org/10.3390/cryst9080395>.
- [33] V. Russo, M. Ghidelli, P. Gondoni, C.S. Casari, A. Li Bassi, Multi-wavelength Raman scattering of nanostructured Al-doped zinc oxide, *J. Appl. Phys.* 115 (2014) 073508. <https://doi.org/10.1063/1.4866322>.
- [34] D. Douth, H.L. Mosbacker, G. Cantwell, J. Zhang, J.J. Song, L.J. Brillson, Impact of near-surface defects and morphology on ZnO luminescence, *Appl. Phys. Lett.* 94 (2009) 042111. <https://doi.org/10.1063/1.3077015>.
- [35] S. Shokhovets, L. Spieß, G. Gobsch, Spectroscopic ellipsometry of wurtzite ZnO and GaN: Examination of a special case, *J. Appl. Phys.* 107 (2010) 023509. <https://doi.org/10.1063/1.3285485>.
- [36] H. Fujiwara, *Spectroscopic ellipsometry: principles and applications*, John Wiley & Sons, Chichester, England ; Hoboken, NJ, 2007.
- [37] G. Malik, S. Mourya, J. Jaiswal, R. Chandra, Effect of annealing parameters on optoelectronic properties of highly ordered ZnO thin films, *Mater. Sci. Semicond. Process.* 100 (2019) 200–213. <https://doi.org/10.1016/j.mssp.2019.04.032>.
- [38] J.M. Khoshman, M.E. Kordesch, Optical constants and band edge of amorphous zinc oxide thin films, *Thin Solid Films*. 515 (2007) 7393–7399. <https://doi.org/10.1016/j.tsf.2007.03.055>.
- [39] F.E. Ghodsi, H. Absalan, Comparative Study of ZnO Thin Films Prepared by Different Sol-Gel Route, *Acta Phys. Pol. A*. 118 (2010) 659–664. <https://doi.org/10.12693/APhysPolA.118.659>.
- [40] D.E. Aspnes, A.A. Studna, E. Kinsbron, Dielectric properties of heavily doped crystalline and amorphous silicon from 1.5 to 6.0 eV, *Phys. Rev. B*. 29 (1984) 768–779. <https://doi.org/10.1103/PhysRevB.29.768>.
- [41] T. Suzuki, S. Adachi, Optical Properties of Amorphous Si Partially Crystallized by Thermal Annealing, *Jpn. J. Appl. Phys.* 32 (1993) 4900–4906. <https://doi.org/10.1143/JJAP.32.4900>.
- [42] D.A.G. Bruggeman, Berechnung verschiedener physikalischer Konstanten von heterogenen Substanzen. I. Dielektrizitätskonstanten und Leitfähigkeiten der Mischkörper aus isotropen Substanzen, *Ann. Phys.* 416 (1935) 665–679. <https://doi.org/10.1002/andp.19354160802>.
- [43] E.N. Epie, W.K. Chu, Ionoluminescence study of Zn- and O- implanted ZnO crystals: An additional perspective, *Appl. Surf. Sci.* 371 (2016) 28–34. <https://doi.org/10.1016/j.apsusc.2016.02.174>.
- [44] B.J. Cowen, M.S. El-Genk, Directional dependence of the threshold displacement energies in metal oxides, *Model. Simul. Mater. Sci. Eng.* 25 (2017) 085009. <https://doi.org/10.1088/1361-651X/aa9193>.
- [45] R. Böttger, L. Bischoff, K.-H. Heinig, W. Pilz, B. Schmidt, From sponge to dot arrays on (100) Ge by increasing the energy of ion impacts, *J. Vac. Sci. Technol. B Nanotechnol. Microelectron. Mater. Process. Meas. Phenom.* 30 (2012) 06FF12. <https://doi.org/10.1116/1.4767269>.
- [46] A. Janotti, C.G. Van de Walle, Native point defects in ZnO, *Phys. Rev. B*. 76 (2007) 165202. <https://doi.org/10.1103/PhysRevB.76.165202>.
- [47] J. Čížek, J. Valenta, P. Hruška, O. Melikhova, I. Procházka, M. Novotný, J. Bulíř, Origin of green luminescence in hydrothermally grown ZnO single crystals, *Appl. Phys. Lett.* 106 (2015) 251902. <https://doi.org/10.1063/1.4922944>.
- [48] A. Azarov, A. Galeckas, C. Mieszczyński, A. Hallén, A. Kuznetsov, Effects of annealing on photoluminescence and defect interplay in ZnO bombarded by heavy ions: Crucial role of the ion dose, *J. Appl. Phys.* 127 (2020) 025701. <https://doi.org/10.1063/1.5134011>.
- [49] G.E. Jellison, P.C. Joshi, Crystalline Silicon Solar Cells, in: H. Fujiwara, R.W. Collins (Eds.), *Spectrosc. Ellipsom. Photovolt.*, Springer International Publishing, Cham, 2018: pp. 201–225. https://doi.org/10.1007/978-3-319-75377-5_8.

